ASTM INTERNATIONAL

Journal of Testing and Evaluation

Kai Wu,[1] Weichen Sun,[2] Songyu Liu,[2] and Haibo Huang[3]

DOI: 10.1520/JTE20190910

# Discrete Element Modeling of Vibration Compaction Effect of the Vibratory Roller in Roundtrips on Gravels

Journal of Testing and Evaluation

doi:10.1520/JTE20190910 available online at www.astm.org

# TECHNICAL NOTE

Kai Wu,[1] Weichen Sun,[2] Songyu Liu,[2] and Haibo Huang[3]

# Discrete Element Modeling of Vibration Compaction Effect of the Vibratory Roller in Roundtrips on Gravels

## Reference

K. Wu, W. Sun, S. Liu, and H. Huang, "Discrete Element Modeling of Vibration Compaction Effect of the Vibratory Roller in Roundtrips on Gravels," *Journal of Testing and Evaluation* https://doi.org/10.1520/JTE20190910

## ABSTRACT

This paper aims to study the vibration compaction mechanism of the vibratory roller on gravels using a two-dimensional discrete element method. The roadbed model was established by gravel particles with irregular shapes, which was closer to reality. The performance parameters of the vibratory roller, such as operating frequency and rolling velocity, were investigated to explore their influences on the operating efficiency of the vibratory roller in roundtrips. The frequencies of 15 Hz and 17 Hz were proved to be the optimal frequency and resonance frequency in the current simulations, respectively. The vibratory roller could achieve a better vibration compaction effect with less power consumption at the optimal frequency. In addition, the number of roundtrips and power consumption should be considered in the selection of the optimal rolling velocity. The movement direction and the contact force distribution of gravels were illustrated by the displacement field, velocity field, as well as the contact force chains. Our results provide a better understanding of the mechanical behavior of gravel particles and their interactions with the vibratory roller.

## Keywords

roller, discrete element method, porosity, optimal frequency, velocity

Manuscript received December 3, 2019; accepted for publication March 13, 2020; published online May 4, 2020.

[1] Transportation School, Southeast University, No. 2 Sipailou, Nanjing C-210096, China (Corresponding author), e-mail: wukai2018@seu.edu.cn, https://orcid.org/0000-0002-9859-8308

[2] Transportation School, Southeast University, No. 2 Sipailou, Nanjing C-210096, China

[3] School of Geography, University College Cork, Western Rd., Cork T12K8AF, Ireland

## Nomenclature

$F_l$, $F_d$ = linear force/dashpot force
$k_r$, $k_s$ = rolling resistance stiffness/shear stiffness
$R_1$, $R_2$ = radius of contacting particle 1/particle 2
$\bar{R}$ = effective radius
$\alpha$ = friction coefficient

$\gamma$ = rolling resistance coefficient
$E^*$ = effective modulus
$\kappa^*$ = normal to shear stiffness ratio
$G$ = weight of the roller
$F_e$ = vibration force
$M$ = eccentric moment
$n$ = porosity
$f$ = vibration frequency
$v$ = rolling speed

## Introduction

Road traffic not only constitutes a pivotal link for connecting cities but also provides an essential channel for the transportation of people, goods, and materials for all sorts of urban development globally. The filling materials of road constructions consist of massive gravels, which are fully compacted during the construction.[1,2] The vibration compaction is a common method that can simultaneously decrease the porosity of gravels and increase the bearing strength of roads.[3] The increase in road density leads to an increase in the bearing capacity of the road. The vibratory roller is considered as one of the most important pieces of construction equipment for road compaction construction. Globally, 85 % of road compaction work is accomplished by the vibratory roller.[4] Therefore, improving the working efficiency of the vibratory roller has become the focus of both academia and industry, as it can not only shorten the road construction period but also improve the equipment utilization rate as well as the road performance. Zhu et al.[5] presented a framework of field construction using intelligent compaction technology together with the assessment of the utilization of the intelligent compaction of roller. Kassem et al.[6] developed a system to monitor and record the compaction mechanism of the roller on site. Wersäll, Nordfelt, and Larsson[7,8] performed full-scale tests to study the influence of the variable operating frequency of the vibratory roller on the compaction of crushed gravel in a controlled environment. However, experimental tests require a lot of workforces, materials, and financial resources, which most laboratories cannot afford. Therefore, numerical simulation is an alternative way to study this subject.

Road construction materials are granular media, the mechanical behaviors of which are influenced by several factors such as sizes, shapes,[9–11] and surface properties.[12,13] Because it is quite difficult to represent these characteristics by the finite element simulation, the discrete element method (DEM), as a specialized methodology for dealing with interactions between discrete element materials, is applied. DEM was first put forward by Cundall and Strack in 1979.[14] This numerical approach can be applied to study the macroscopic and microscopic behaviors of granular media simultaneously.[15–17] Dondi et al.[18] simulated asphalt mixtures using the viscoelastic burger contact model. Ma et al.[19] conducted the DEM simulation of wheel tracking tests to predict the rutting deformation of asphalt mixtures and explained the reason. Jia et al.[20] investigated the macro- and micro-mechanisms of granular particles during the dynamic compaction process, revealing two stages of dynamic compaction, i.e., compaction caused by the transient impact and the vibration compaction. One research that focused on the wheel–soil interaction was conducted by Jiang et al.,[21] aiming to better understand the tractive efficiency and rover performance in the lunar environment. Although a handful of papers have studied the related topics, little attention has been paid to either the operating efficiency of the vibratory roller or the mechanical behavior of granular particles under the dynamic vibration compression. Most of the related simulations simplify the movement of the vibratory roller by fixing the vibration position without considering the driving movement and rolling behavior of the vibratory roller, not to mention the back and forth compaction of the vibratory roller on a section of the roadbed.

The present paper aims to study the working mechanism of the vibratory roller in roundtrips on gravels both from macroscopic and microscopic views through two-dimensional (2D) DEM simulations. We focused on the

influences of the optimal frequency and optimal velocity of the roller on the vibration compaction results of the gravels. It is proved that the vibratory roller could achieve a better vibration compaction effect with less power consumption when compacting at the optimal frequency and moving with an optimal velocity. The following section introduces the roadbed model composed of gravel particles in irregular shapes and the motion law of the vibratory roller. The Results and Discussion section presents the calibration of the DEM model and then investigates the machine performance parameters of the roller, such as frequency and moving speed. The microscopic behaviors of gravel particles and vibration compaction effects, including the contact force chain, particle displacement field, as well as the velocity field of gravels materials, were plotted. Finally, the discussion and the main findings of this paper were elaborated.

## DEM Simulation Process

### CONTACT LAW

In this paper, the software Particle Flow Code 5.0 (PFC5.0, Itasca Company, IL, USA) was used for the simulation. The rolling resistance linear model was applied.[22–24] The contact law considered the torque acting on the contacting pieces to counteract rolling motion. The internal moment increases linearly with the accumulated relative rotation of the contacting pieces at the contact point. The force-displacement law for the rolling resistance linear model updates the contact force and moment, as shown in equation (1):

$$F = F_l + F_d \tag{1}$$

where $F_l$ is the linear force and $F_d$ is the dashpot force.

The rolling resistance moment $M_r$ is incremented in equation (2):

$$M_r = M_r - k_r \Delta\theta_b \tag{2}$$

where $\Delta\theta_b$ is the relative bend-rotation increment.

The rolling resistance stiffness $k_r$ is calculated in equation (3):

$$k_r = k_s \bar{R}^2 \tag{3}$$

where $k_s$ is the shear stiffness.

The normal and tangential stiffness can be calculated by the effective modulus $E^*$ and normal to shear stiffness ratio $\kappa^*$ at the contact in equations (4) and (5),[25] respectively.

$$k_n = \frac{AE^*}{L} \tag{4}$$

$$k_s = \frac{k_n}{\kappa^*} \tag{5}$$

where $A$ is the surface area of the particle and $L$ is the distance between the center of two contacting particles.

The contact effective radius $\bar{R}$ is calculated in equation (6)[25]:

$$\frac{1}{\bar{R}} = \frac{1}{R_1} + \frac{1}{R_2} \tag{6}$$

where $R_1$ and $R_2$ are radii of contacting particles, respectively.

The rolling resistance moment $M_r$ is updated, but it cannot exceed the limiting torque $M_{limit}$ calculated in equation (7):

$$M_{limit} = \mu_r \bar{R} F_l^n \tag{7}$$

where the rolling resistance coefficient $\mu_r$ corresponds to the tangent of the maximum angle of a slope where the rolling resistance torque counterbalances the torque produced by gravity on the particle.

## DEM SIMULATION OF ROLLER

A general acknowledgment is made that there exist differences between 2D and three-dimensional (3D) numerical simulations. The stress state in 2D is likely to be different from the real 3D case in terms of particle shape, selection of parameters, and spatial arrangement of discs/particles. Nevertheless, our research aimed to explain the vibration compaction mechanism of the roller on the gravels. Because the roller mainly moves in-plane in the roundtrip movement, the 2D simulation of the roller is suitable in this case. Starting with a simulation in 2D can simplify the spatial relationships of particles, facilitate computer programming, as well as reduce the computation time.

The DEM simulation of the roller was performed based on the full-scale experimental tests of soil compaction by vibratory roller presented in Wersäll, Nordfelt, and Larsson.[7,8] Soil is a kind of well-graded gravel. The particle size distribution curves of Wersäll, Nordfelt, and Larsson[7] and DEM simulations are presented in figure 1, changing the log coordinate of the abscissa to the natural number coordinate. Due to the limitation of computer calculation performance, the gradation curve in DEM simulation shifts to the right to enlarge the particle size, reducing the number of particles. The dry density of soil is 2,230 kg/m$^3$. The initial porosity in 3D is calculated as shown in equation (8):

$$n = 1 - \frac{\rho_0}{\rho} \tag{8}$$

where $\rho_0$ is apparent density and $\rho$ is dry density. The initial porosity in Wersäll, Nordfelt, and Larsson[7,8] was calculated to be 0.42.

**FIG. 1**

The particle size distribution of Wersäll, Nordfelt, and Larsson[7,8] and DEM simulations.

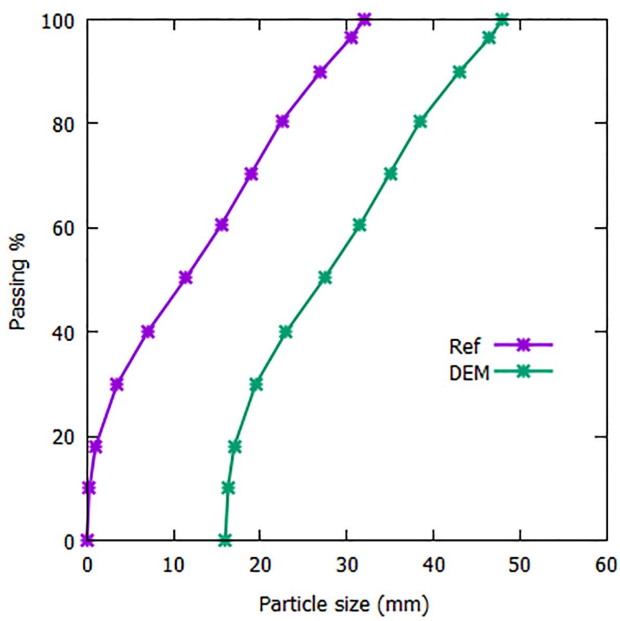

Wang et al.[26] proposed the equation (9) to convert the porosity from 3D to 2D

$$n_{2d} = 0.42 \times n_{3d}^2 + 0.25 \times n_{3d} \tag{9}$$

Therefore, the porosity in 2D can be determined to be 0.18 from the porosity of 0.42 in 3D.

The first step of the simulation involves the preparation of the roadbed model. It is well known that particle shapes play a critical role in the mechanical behavior of gravels.[27–29] To make the simulation as close to reality as possible, gravel materials were represented with particle templates with different shapes. Particles smaller than 31 mm are generated from the template of two overlapping discs. The large-sized particles are generated from a total of 25 templates with irregular shapes by random selection. The whole particle templates are shown in **figure 2**. Each template is composed of discs of different sizes and numbers. The boundary lines shown in the first template of large size illustrates how the template is constituted of discs. The dimension of the whole roadbed model is 7.0 × 1.0 m, containing about 20,000 gravel particles. The x-axis ranges between −1.0 and 6.0 m. The roller moves in the range of 0.0 to 5.0 m, leaving two sections of −1.0 to 0 m and 5.0 to 6.0 m from the stiff boundary effects.[30] **Figure 3** illustrates the entire model, in which a small part of the sample is enlarged to show the compositions of gravel particles with irregular forms. The micro-mechanical parameters are presented in **Table 1**.[26–28]

The key vibration component of the vibratory roller was simulated by a simplified large disc in 2D with a diameter of 1.52 m. The mass of the roller was set to be 7,600 kg. The vibratory roller generally moved in three ways: horizontal movement, vibration, and rolling. In the horizontal direction, the roller moved forth and back

**FIG. 2**

Gravel templates with irregular shapes.

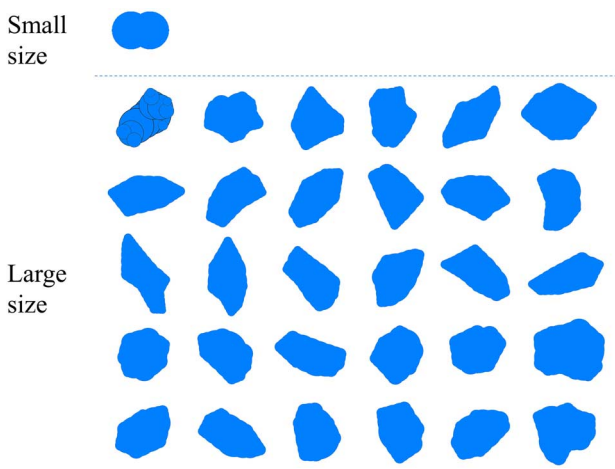


**FIG. 3**

DEM model of roadbed composed of gravels with irregular shapes.

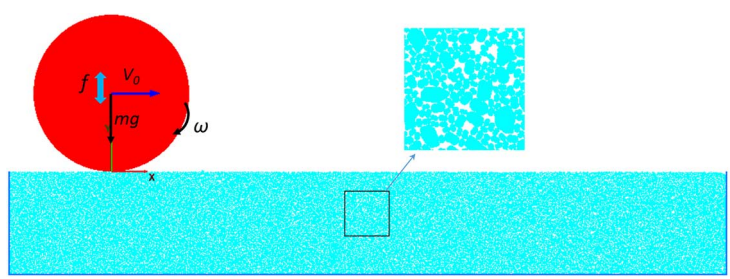

**TABLE 1**
Default parameters of gravel used in the DEM simulation of the roller

| Parameter | Value | Unit |
|---|---|---|
| Effective modulus, $E^*$ | 50 | MPa |
| Normal to shear stiffness ratio, $\kappa^*$ | 1.0 | … |
| Normal critical damping ratio, $\beta_n$ | 0.2 | … |
| Shear critical damping ratio, $\beta_s$ | 0.2 | … |
| Density | 2,230 | kg/$m^3$ |
| Damping | 0.7 | … |
| Friction coefficient, $\alpha$ | 0.5 | … |
| Rolling resistance coefficient, $\gamma$ | 0.3 | … |
| Time step, Δt | $1 \times 10^{-5}$ | s/step |
| Gravitational acceleration, $g$ | 9.8 | m/$s^2$ |

between the starting point (0.0, 0.0) and the endpoint (5.0, 0.0). In the vertical direction, the roller vibrated at a specific frequency, $f$. The vibration force applied on the roller was the sum of the static force of the vibrating wheel and the dynamic force of the vibration component, as calculated in equation (10):

$$F = G + F_e \tag{10}$$

where $F$ is the vibration force, $G$ is the weight of the roller, and $f$ is the vibration frequency. $F_e$ is the maximum value of the vibration force, as calculated in equation (11):

$$F_e = \mathrm{M} \times (2\pi f)^2 \tag{11}$$

where M is the eccentric moment, which is set as 7.38 kgm.[7]

Furthermore, the angular velocity of the roller was not fixed in the present simulations. Thus, the roller could roll on the roadbed surface. Besides, the rolling and squeezing of the roller on the gravels could be observed in the simulation.

The measuring circles were used to monitor parameter changes along with the roller movements. Three rows of measuring circles were positioned in the roadbed model, as shown in **figure 4**. After the pretest, the radius of the measuring circle was set to be 0.22 m, so that the upper measuring circles were always full of gravel particles (the gravel particles on the roadbed surface could be squeezed out of the measuring circle in larger dimension due to the rolling effect of the vibrating roller). Three rows of measuring circles made it possible to monitor the evolution of the porosity of the upper/middle/bottom layers of soils with different depths. The porosity $n$ in the corresponding measuring circle is calculated in the following equation (12):

**FIG. 4**
Three rows of the measuring circles to monitor the porosities of the upper/middle/bottom layers of soils.

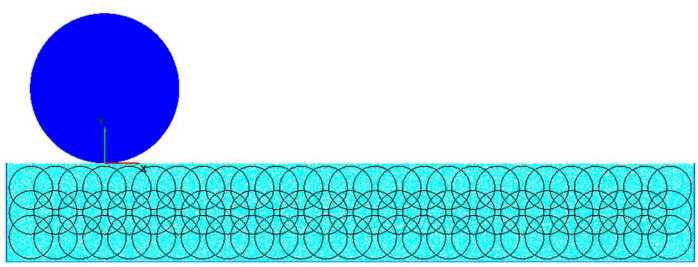

$$n = \frac{V_{void}}{V_{circle}} = 1 - \frac{V_{mat}}{V_{circle}} \tag{12}$$

where $V_{mat}$ represents the surface of gravels in the target measuring circle and $V_{circle}$ represents the surface of the measuring circle.

Figure 5 presents the deformation of the road surface in eight roundtrips of the vibratory roller. In the beginning, the road surface was flat. After one roundtrip, it started to deform gradually. Two roundtrips later, the middle part of the road was compacted and settled. Four roundtrips later, slight protrusions appeared on both sides of the road because the roller was unable to roll out of the boundary, leaving the protruding zone generally difficult to be compacted. After eight roundtrips, the middle section of the roadbed was more compacted than the initial state.

During a roundtrip of the vibrating roller movement, the porosity variation presented a typical tendency, as shown in figure 6. The x-axis of the curve represents the length of the roadbed model, while the y-axis represents the porosity variation. In one roundtrip, when the roller started to compact the roadbed, the porosity remained constant because the vibration effect on the gravel materials had not yet influenced the target measurement

**FIG. 5**

Surface deformation of gravel materials in eight roundtrips.

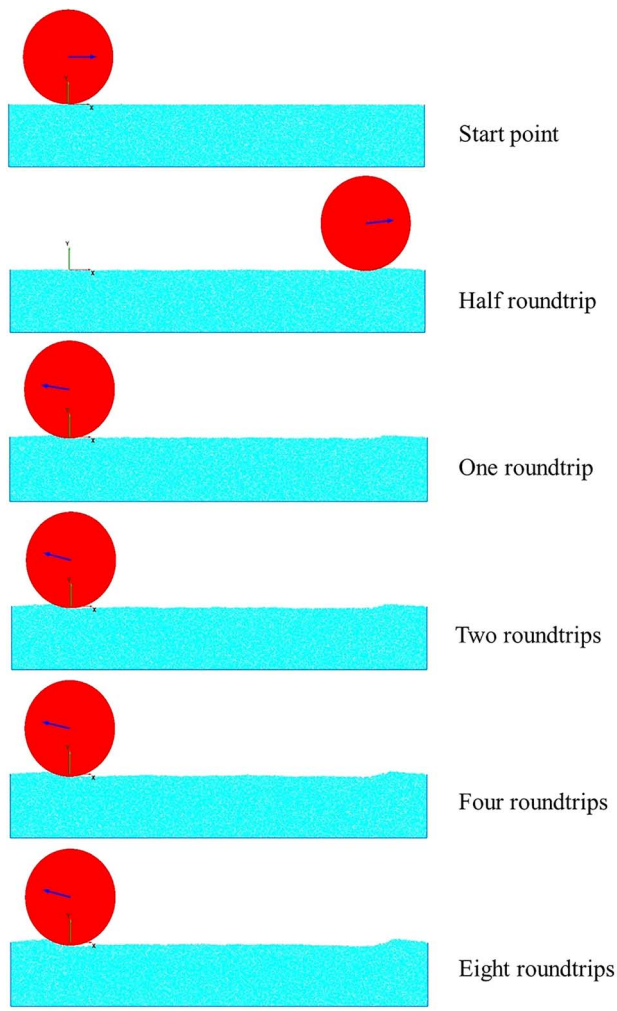

**FIG. 6**

The typical tendency of porosity variation according to the distance of gravel materials in a measuring circle during a round trip of the vibratory roller movement.

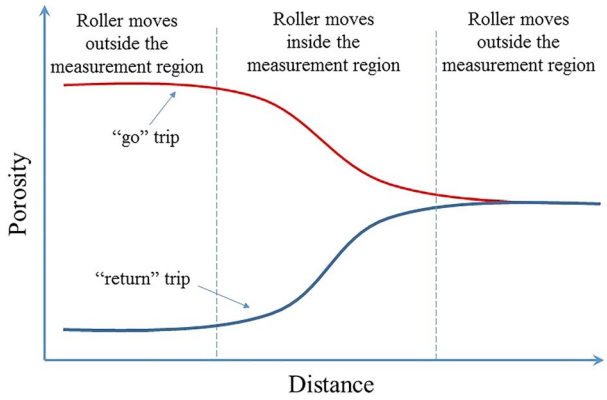


region. When the roller moved inside the target measurement region, the porosity decreased because of the vibration compaction effect. When the roller left the target measurement region, the porosity remained constant again until the roller re-entered the target measurement region. Then, the porosity continued to decrease. It should be noted that the porosity curve suddenly rises for the measuring circles in the upper row, resulting from the fact that the roller pushes or squeezes the granular soils out of the measuring circle. Nevertheless, this phenomenon is mitigated in the middle layer and disappears in the bottom layer of the soil. Overall, the upper, middle and bottom soil layers have been monitored simultaneously to draw the general conclusion.

## Results and Discussion

### COMPARISON BETWEEN EXPERIMENTAL TEST AND NUMERICAL SIMULATION

The numerical simulations were firstly compared with the full-scale experimental tests performed in Wersäll, Nordfelt, and Larsson.[7] Figure 7 shows the settlement of the soil surface in a roundtrip at different frequencies

**FIG. 7**

Comparisons of settlement between full-scale experiments and numerical simulations.

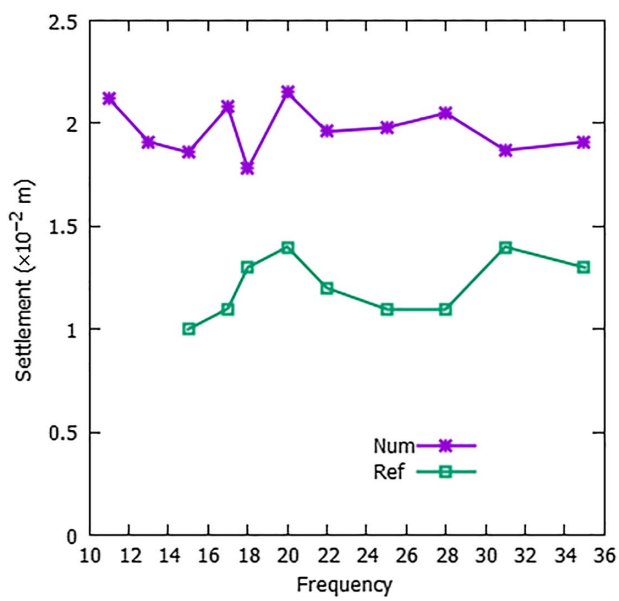

of $f = 11$, 13, 15, 17, 18, 20, 22, 25, 28, 31, and 35 Hz. After one roundtrip, the settlement obtained from simulations was about 2 cm, which was close to that of 1.2 cm in the experimental tests. The discrepancy was probably due to the movements of the roller, including one static pass at a speed of 0.35 m/s and two vibrating passes at the frequency of 28 Hz over the roadbed surface before the format fixed-frequency experimental tests, suggesting that the soil had already been compacted to a certain extent. In addition, the current 2D DEM simulation of vibratory roller aimed to explain the vibration compaction mechanism of the roller on the gravel particles, which is a supplement to the understanding of the experimental tests rather than a prediction of the experimental results. In addition, the simulation in 2D can simplify the spatial relationships of particles, facilitate computer programming, and reduce the computation time. Therefore, it is feasible to apply DEM to simulate the vibratory roller in 2D.

## INFLUENCE OF VIBRATORY ROLLER PARAMETERS

### Influence of Frequency

The vibration frequency is considered one of the most important parameters for the roller performance. Wersäll, Nordfelt, and Larsson[7] indicated that there is an optimal frequency of roller operation, at which the roller performs better vibration compaction with less fuel consumption and extended roller life. Steyn and Reynolds[31] monitored both the frequencies inside the materials and on the roller drum, and compared with the frequencies applied in the laboratory on the vibration table from three different base layer materials. Their results indicated the importance of selecting appropriate frequencies for different types of road-building materials to enable optimal compaction. In this section, the vibration effects of the vibratory roller in a single roundtrip at 11 different frequencies of $f = 11$, 13, 15, 17, 18, 20, 22, 25, 28, 31, and 35 Hz were investigated. Figure 8 shows the evolution of the porosity of the upper layer compacted by the roller at different frequencies in a roundtrip. All the curves start from the same initial point of 0.181. Because the particles in the upper layer were easily shaken out of the measuring circles, the curves rose to a peak value of about 0.20 and then declined. After one roundtrip of vibration compaction, the optimal final porosity decreased to 0.171, which was obtained at the frequency of 22 Hz. Among other frequencies, the final porosity at the frequency of 15 Hz was about 0.174, not far from the final porosity of 22 Hz. Interestingly, the final porosity at 17 Hz after one roundtrip compaction was larger than the initial porosity. It is supposed that 17 Hz is the resonance frequency of the gravel and the roller. The resonance loosened the soil, leading to the loose surface layer of the soil after the vibration compaction at 17 Hz in a roundtrip.

**FIG. 8**

Evolution of porosity of the upper layer of soil compacted by the roller at different frequencies in a roundtrip.

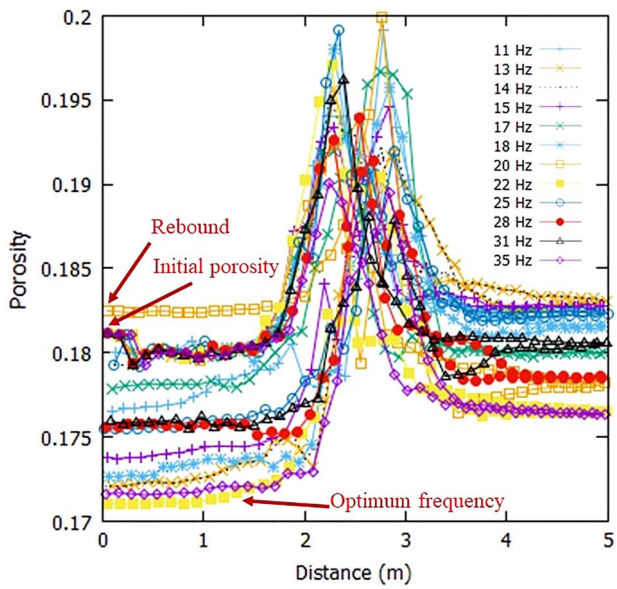

Figure 9 exhibits the evolution of the porosity of the middle layer compacted by a roller at different frequencies in a roundtrip. The optimal final porosity was about 0.167, which was obtained at frequencies of 15 Hz and 28 Hz. Considering the power consumption of the roller, 15 Hz is determined as the optimal frequency for vibration compaction of the middle layer. The worst vibration compaction effects were obtained at 11 Hz and 17 Hz. The poor effect of 11 Hz was due to the low power of the roller, while that of 17 Hz was due to the resonance.

Figure 10 presents the evolution of the porosity of the bottom layer compacted by a roller at different frequencies in a roundtrip. The optimal final porosity was about 0.170, which was obtained at the frequencies

**FIG. 9**

Evolution of porosity of the middle layer of soil compacted by the roller at different frequencies in a roundtrip.

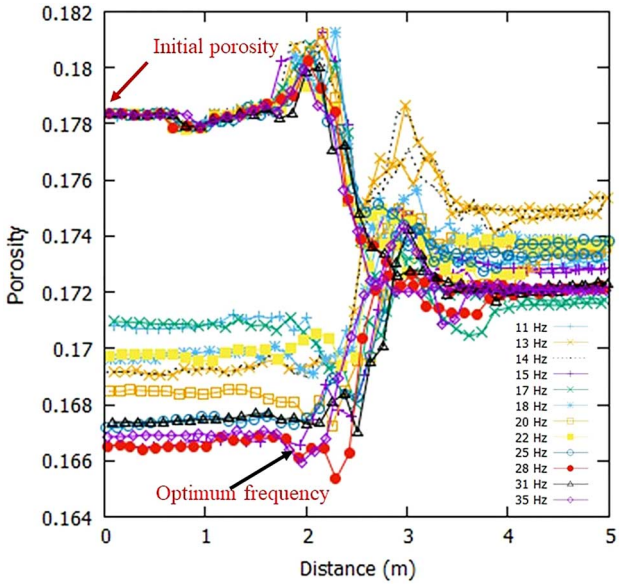


**FIG. 10**

Evolution of porosity of the bottom layer of soil compacted by the roller at different frequencies in a roundtrip.

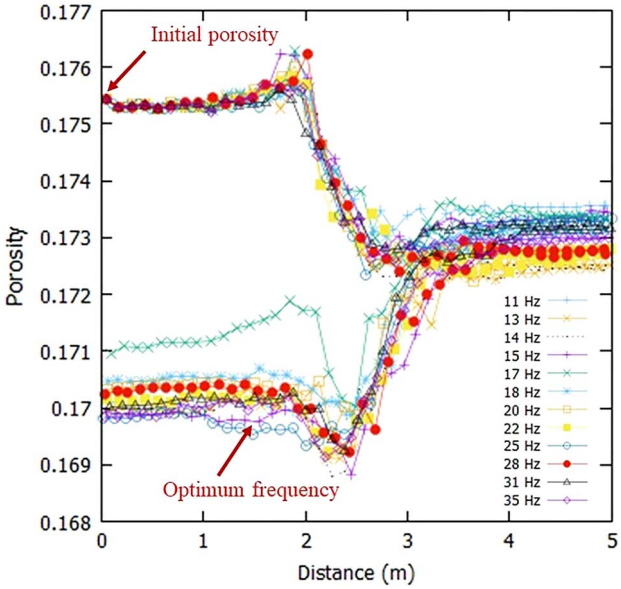

**FIG. 11**

Relationship between the final porosity and frequency of the upper, middle, and bottom layers in one roundtrip.

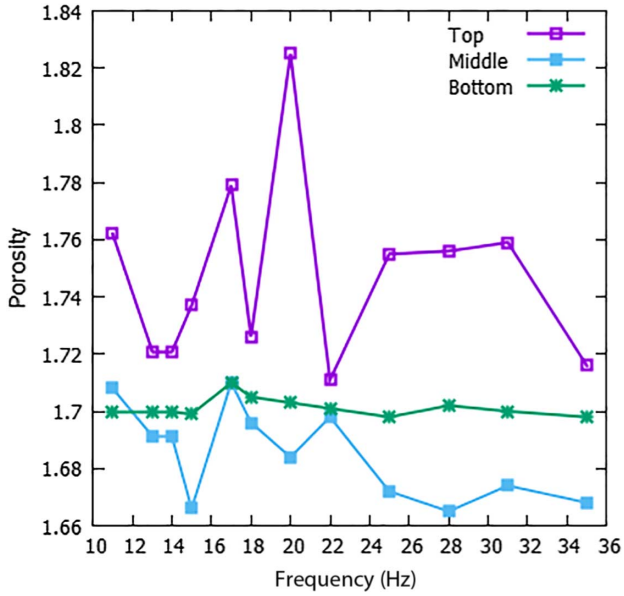


of 15, 25, and 35 Hz. Considering the power consumption, 15 Hz was the optimal frequency. Due to the resonance, the effect of 17 Hz was the worst, 6 % less than that of the optimal frequency. Besides, the peak values significantly reduced or nearly disappeared compared with the curves of the upper layer.

To sum up, the frequencies of 15 Hz and 17 Hz are the optimal frequency and the resonance frequency in current simulations, respectively. In comparison, Wersäll, Nordfelt, and Larsson[7] reported that 18 Hz and 17 Hz were the optimal frequency and the resonance frequency in their experiments, respectively. In our opinion, the resonance frequency is an intrinsic property of the granular materials, while the optimal frequency is influenced by the particle sizes. Therefore, our resonance frequency is the same as theirs, while our optimal frequency is slightly smaller than their finding, because the particle sizes are greater than that in their experiments. However, we agree with Wersäll, Nordfelt, and Larsson[7] that the optimal frequency is very close to the resonance frequency.

Figure 11 exhibits the relationship between the final porosity and the frequency for the upper, middle, and bottom layers in a roundtrip. There are three points worth noting: (1) the fluctuations of porosity with different frequencies for different layers are different due to the effect of vibratory compaction decreases with depth, exhibiting that the upper porosity fluctuates greatly under vibration compaction, while the bottom layer shows the smallest fluctuation; (2) the final porosity of the middle layer is smaller than that of the bottom layer after the vibration compaction; (3) the porosity first decreases until the optimal frequency and then increases. After reaching the resonance frequency, the porosity decreases again with an increase of the frequency, owing to the increase of power consumption.

## Influence of Roller Velocity

The moving velocity of the vibratory roller affects the operating efficiency. When the roller moves slowly, the vibration can be applied to one position, completely transferring the vibration energy to the ground. On the contrary, when the roller moves fast, the compaction effect of a single roundtrip weakens, while the number of rolling operations within the same time increases. Therefore, the optimal velocity can not only improve the construction quality but also accelerate the construction progress. The following study on the influence of rolling velocities was carried out at the optimal frequency of 15 Hz.

Figures 12–14 present the evolution of porosity of the gravels in the upper/middle/bottom layers at four different rolling velocities of $v_1 = 0.5$ m/s, $v_2 = 1.0$ m/s, $v_3 = 2.0$ m/s, and $v_4 = 4.0$ m/s during the same operation time of 10 s. Correspondingly, the numbers of roundtrips are 0.5, 1.0, 2.0, and 4.0, respectively. Taking the porosity of middle layer as an example, the final porosities at different velocities of 0.5, 1.0, 2.0, and 4.0 m/s are 0.162, 0.167, 0.169, and 0.171, respectively. It could be observed that the vibration effect weakened as the rolling velocity increased. The porosity at the rolling velocity of $v_1$ decreased from 0.178 to 0.163, showing an approximately 9.9 % enhancement, while that at the rolling velocity of $v_4$ decreased from 0.178 to 0.171, with an approximately 4.0 %

**FIG. 12**

Evolution of porosity of the upper layer of soil compacted by the roller with different rolling speeds working in the same period of time.

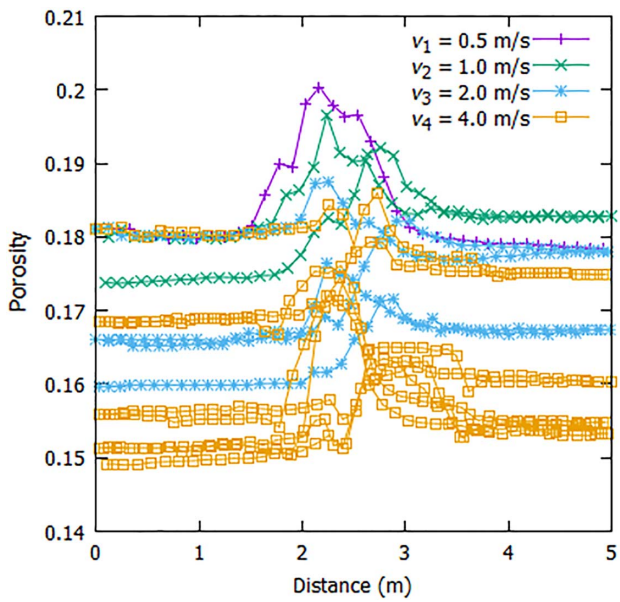


**FIG. 13**

Evolution of porosity of the middle layer of soil compacted by roller with different rolling velocities working in the same period of time.

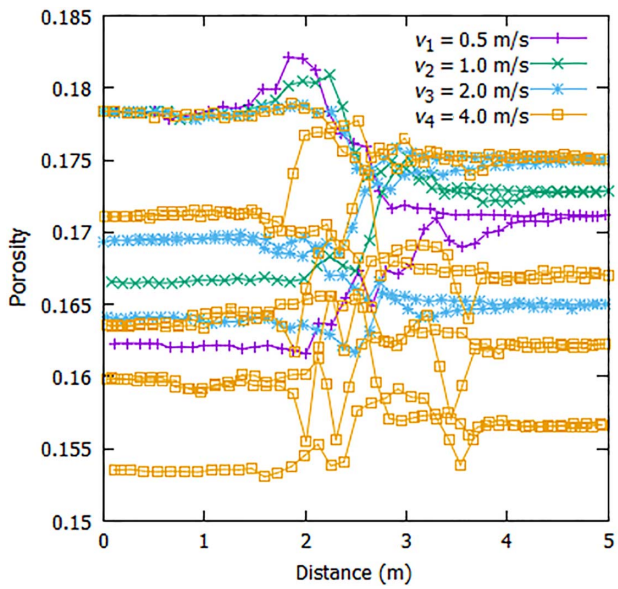

**FIG. 14**

Evolution of porosity of the bottom layer of soil compacted by roller with different rolling velocities working in the same period of time.

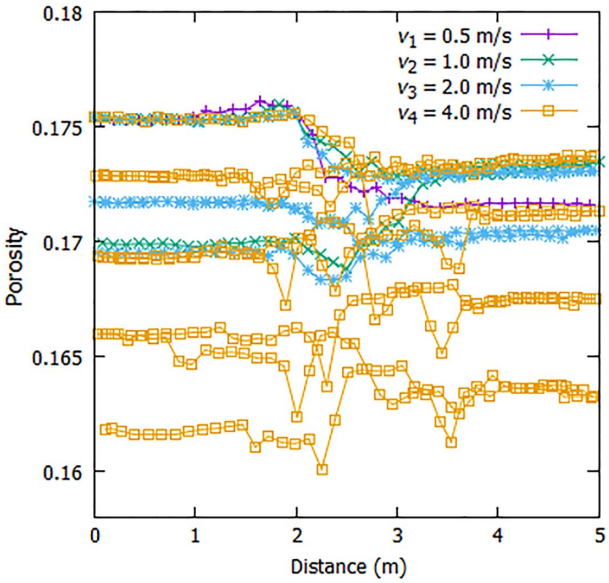


enhancement. In this case, the compaction effect of the single roundtrip at the rolling velocity of $v_1$ can be regarded as the optimum. However, the situation changed as the number of roundtrips increased. Figure 13 reveals the evolution of porosity within the same operation time (10 s) at different rolling velocities. The final porosities at four velocities were 0.171, 0.167, 0.164, and 0.153, respectively. When the roller finished four roundtrips at a velocity of $v_4 = 4$ m/s, the roller with a lower speed of $v_1 = 0.5$ m/s finished only half of the roundtrip. As a result, the final porosity of curve $v_4$ decreased to 0.153, much better than 0.171 of the curve $v_1$. Therefore, the velocity of $v_4$ is more efficient in this case. It is noteworthy that more roundtrips cost more fuel. Therefore, the optimal choice of rolling velocities should consider both the number of roundtrips and power consumption.

## MICROSCALE RESULTS

### Displacement Field

The evolution of the displacement field of gravels during the first vibration compaction is exhibited in figure 15. The color of the displacement changes as the depth changes, suggesting that the vibration compaction effect of the roller declines gradually.

**FIG. 15**

The displacement field of gravel materials under the vibration compression of the vibratory roller.

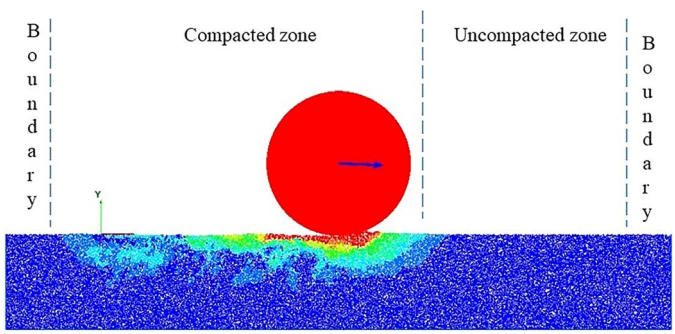

**FIG. 16**

The direction of the displacement vector of gravel materials under the vibration compression of the vibratory roller.

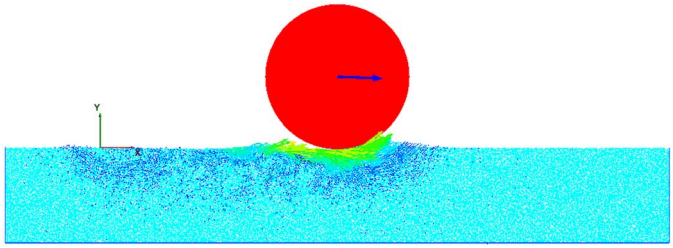


**FIG. 17**

Velocity field of gravel materials under the vibration compression of the vibratory roller.

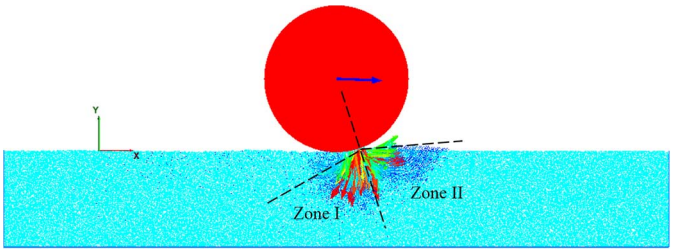


In figure 16, the moving direction of the gravels is presented by the displacement vector. With the roller moving from left to right, the gravels passed by the roller moved towards the bottom right. However, due to the obstruction of gravel materials ahead, the gravels currently under the roller moved towards the upper right direction, which forced some of the gravels to move upward only. A similar phenomenon is also observed in figure 17.

## Velocity Field

Figure 17 presents the velocity vector of the gravel materials. It can be noted that the velocity of gravels under the roller is higher than those in other zones. The moving direction of the gravels can be divided into two zones: downwards in Zone I and toward the upper right in Zone II. The gravels in Zone II are more likely to be squeezed out.

## Contact Force Chains

The DEM simulation is a powerful tool for plotting the contact force chain, which is a basic microscopic static variable between gravels. The contact force chain plot is of great help to study energy transmission across the entire roadbed model. The magnitude of contact forces is typically uneven. The more distinct and strong the force chains, the more stress they carry.[32] Two significant features should be noted in figure 18: (i) the strong force network plays an important role in the interaction between the roller and the gravels, and (ii) the contact

**FIG. 18**

Contact force chains between gravel materials under the vibration compression of the vibratory roller.

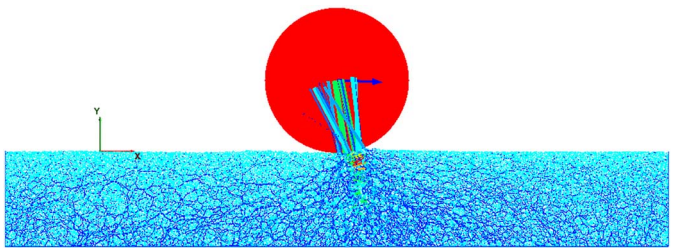

force chain diffuses from the contact point to the depth of the entire model. The force chain distributes the contact force to the gravels in a triangular form under the roller.

## Conclusions

This research proposes a novel 2D DEM simulation of the vibratory roller to study the vibration compaction mechanism on gravels in roundtrips. The establishment of the roadbed model with irregular shapes made our simulation closer to the actual situation. Our research specifically emphasized the effect of mechanical characteristics of gravels as well as the operating parameters of the roller on the compaction vibration. The simulations were validated by experimental tests. Based on the numerical simulation findings discussed previously, the following conclusions can be drawn:

1. The vibratory roller compacting at the optimal frequency performed a better vibration compaction effect with less power consumption. The frequencies of 15 Hz and 17 Hz were the optimal frequency and the resonance frequency in current simulations, respectively. The optimal frequency was proved to be very close to the resonance frequency.
2. Although slower rolling velocity achieved better vibration compaction effect in a single roundtrip, increasing the number of roundtrips by accelerating the velocity achieved a better compaction effect within the same operation time. However, more roundtrips mean more power consumption. Therefore, the optimal choice of rolling velocities should also consider the number of roundtrips and power consumption.
3. The displacement field, velocity field, and contact forces show the interaction mechanism between the roller and gravels during the vibration compaction process. The movement directions of gravels under the roller were typically divided into two directions, and the strong force network played an important role in the interaction between the roller and the granular particles.

In future research, we will further explore the relationships between the optimal frequency and the optimal speed, as well as the influence of the different materials based on the DEM simulations of roller.

#### ACKNOWLEDGMENTS

We gratefully acknowledge the financial support provided by the National Natural Science Foundation of China No. 51608112, the National Key Research and Development Program of China No. 2016YFC0800201, and the Fundamental Research Funds for the Central Universities No. 2242019k30039.

## References

1. I. Rodríguez-Fernández, P. Lastra-González, I. Indacoechea-Vega, and D. Castro-Fresno, "Recyclability Potential of Asphalt Mixes Containing Reclaimed Asphalt Pavement and Industrial By-Products," *Construction and Building Materials* 195 (January 2019): 148–155, https://doi.org/10.1016/j.conbuildmat.2018.11.069
2. T. B. Moghaddam and H. Baaj, "Rheological Characterization of High-Modulus Asphalt Mix with Modified Asphalt Binders," *Construction and Building Materials* 193 (December 2018): 142–152, https://doi.org/10.1016/j.conbuildmat.2018.10.194
3. J. Kodikara, T. Islam, and A. Sounthararajah, "Review of Soil Compaction: History and Recent Developments," *Transportation Geotechnics* 17, part B (December 2018): 24–34, https://doi.org/10.1016/j.trgeo.2018.09.006
4. H. Zhang, "Study on the Compaction Mechanism of the Hydraulic Single Steel Wheel Vibratory Roller" (PhD thesis, Chang'an University, 2016).
5. X. Zhu, S. Bai, G. Xue, J. Yang, Y. Cai, W. Hu, X. Jia, and B. Huang, "Assessment of Compaction Quality of Multi-Layer Pavement Structure Based on Intelligent Compaction Technology," *Construction and Building Materials* 161 (February 2018): 316–329, https://doi.org/10.1016/j.conbuildmat.2017.11.139
6. E. Kassem, W. Liu, T. Scullion, E. Masad, and A. Chowdhury, "Development of Compaction Monitoring System for Asphalt Pavements," *Construction and Building Materials* 96 (October 2015): 334–345, https://doi.org/10.1016/j.conbuildmat.2015.07.041
7. C. Wersäll, I. Nordfelt, and S. Larsson, "Soil Compaction by Vibratory Roller with Variable Frequency," *Géotechnique* 67, no. 3 (2017): 272–278, https://doi.org/10.1680/jgeot.16.P.051

8. C. Wersäll, I. Nordfelt, and S. Larsson, "Resonant Roller Compaction of Gravel in Full-Scale Tests," *Transportation Geotechnics* 14 (March 2018): 93–97, https://doi.org/10.1016/j.trgeo.2017.11.004
9. J. Zheng and R. D. Hryciw, "Roundness and Sphericity of Soil Particles in Assemblies by Computational Geometry," *Journal of Computing in Civil Engineering* 30, no. 6 (2016): 04016021, https://doi.org/10.1061/(ASCE)CP.1943-5487.0000578
10. G. Dondi, A. Simone, V. Vignali, and G. Manganelli, "Numerical and Experimental Study of Granular Mixes for Asphalts," *Powder Technology* 232 (December 2012): 31–40, https://doi.org/10.1016/j.powtec.2012.07.057
11. S. J. Lee, Y. M. A. Hashash, and E. G. Nezami, "Simulation of Triaxial Compression Tests with Polyhedral Discrete Elements," *Computers and Geotechnics* 43 (June 2012): 92–100, https://doi.org/10.1016/j.compgeo.2012.02.011
12. J. Härtl and J. Y. Ooi, "Numerical Investigation of Particle Shape and Particle Friction on Limiting Bulk Friction in Direct Shear Tests and Comparison with Experiments," *Powder Technology* 212, no. 1 (2011): 231–239, https://doi.org/10.1016/j.powtec.2011.05.022
13. F. Göncü and S. Luding, "Effect of Particle Friction and Polydispersity on the Macroscopic Stress–Strain Relations of Granular Materials," *Acta Geotechnica* 8, no. 6 (2013): 629–643, https://doi.org/10.1007/s11440-013-0258-z
14. P. A. Cundall and O. D. L. Strack, "A Discrete Numerical Model for Granular Assemblies," *Géotechnique* 29, no. 1 (1979): 47–65, https://doi.org/10.1680/geot.1979.29.1.47
15. C. O'sullivan, *Particulate Discrete Element Modelling* (Boca Raton, FL: CRC Press, 2011).
16. Y. He and F. Guo, "Micromechanical Analysis on the Compaction of Tetrahedral Particles," *Chemical Engineering Research and Design* 136 (August 2018): 610–619, https://doi.org/10.1016/j.cherd.2018.06.019
17. Z. Zhang, X. Zhang, H. Qiu, and M. Daddow, "Dynamic Characteristics of Track-Ballast-Silty Clay with Irregular Vibration Levels Generated by High-Speed Train Based on DEM," *Construction and Building Materials* 125 (October 2016): 564–573, https://doi.org/10.1016/j.conbuildmat.2016.08.079
18. G. Dondi, V. Vignali, M. Pettinari, F. Mazzotta, A. Simone, and C. Sangiorgi, "Modeling the DSR Complex Shear Modulus of Asphalt Binder Using 3D Discrete Element Approach," *Construction and Building Materials* 54 (March 2014): 236–246, https://doi.org/10.1016/j.conbuildmat.2013.12.005
19. T. Ma, D. Zhang, Y. Zhang, and J. Hong, "Micromechanical Response of Aggregate Skeleton within Asphalt Mixture Based on Virtual Simulation of Wheel Tracking Test," *Construction and Building Materials* 111 (May 2016): 153–163, https://doi.org/10.1016/j.conbuildmat.2016.02.104
20. M. Jia, Y. Yang, B. Liu, and S. Wu, "PFC/Flac Coupled Simulation of Dynamic Compaction in Granular Particles," *Granular Matter* 20, no. 4 (2018): 76, https://doi.org/10.1007/s10035-018-0841-y
21. M. Jiang, Y. Dai, L. Cui, and B. Xi, "Experimental and DEM Analyses on Wheel-Soil Interaction," *Journal of Terramechanics* 76 (April 2018): 15–28, https://doi.org/10.1016/j.jterra.2017.12.001
22. K. Iwashita and M. Oda, "Micro-deformation Mechanism of Shear Banding Process Based on Modified Distinct Element Method," *Powder Technology* 109, nos. 1–3 (2000): 192–205, https://doi.org/10.1016/S0032-5910(99)00236-3
23. M. Oda and K. Iwashita, "Study on Couple Stress and Shear Band Development in Granular Media Based on Numerical Simulation Analyses," *International Journal of Engineering Science* 38, no. 15 (2000): 1713–1740, https://doi.org/10.1016/S0020-7225(99)00132-9
24. K. Wu, P. Pizette, F. Becquart, S. Rémond, N. Abriak, W. Xu, and S. Liu, "Experimental and Numerical Study of Cylindrical Triaxial Test on Mono-Sized Glass Beads under Quasi-static Loading Condition," *Advanced Powder Technology* 28, no. 1 (2017): 155–166, https://doi.org/10.1016/j.apt.2016.09.006
25. J. Liu, "A Dynamic Modelling Method of a Rotor-Roller Bearing-Housing System with a Localized Fault Including the Additional Excitation Zone," *Journal of Sound and Vibration* 469 (March 2020): 115144, https://doi.org/10.1016/j.jsv.2019.115144
26. Z. Wang, A. Ruiken, F. Jacobs, and M. Ziegler, "A New Suggestion for Determining 2D Porosities in DEM Studies," *Geomechanics and Engineering* 7, no. 6 (2014): 665–678, https://doi.org/10.12989/gae.2014.7.6.665
27. S. Zhao and X. Zhou, "Effects of Particle Asphericity on the Macro- and Micro-mechanical Behaviors of Granular Assemblies," *Granular Matter* 19, no. 2 (2017): 38, https://doi.org/10.1007/s10035-017-0725-6
28. Y. Lu, Y. Tan, X. Li, and C. Liu, "Methodology for Simulation of Irregularly Shaped Gravel Grains and Its Application to DEM Modeling," *Journal of Computing in Civil Engineering* 31, no. 5 (2017): 04017023, https://doi.org/10.1061/(ASCE)CP.1943-5487.0000676
29. M. Khanal, M. Elmouttie, and D. Adhikary, "Effects of Particle Shapes to Achieve Angle of Repose and Force Displacement Behaviour on Granular Assembly," *Advanced Powder Technology* 28, no. 8 (2017): 1972–1976, https://doi.org/10.1016/j.apt.2017.04.016
30. L. Zhang and T. M. Evans, "Boundary Effects in Discrete Element Method Modeling of Undrained Cyclic Triaxial and Simple Shear Element Tests," *Granular Matter* 20, no. 4 (2018): 60, https://doi.org/10.1007/s10035-018-0832-z
31. W. J. Steyn and G. Reynolds, "Evaluation of Optimal Compaction Frequencies for Granular Materials," in *GeoChina 2016: Advances in Pavement Engineering and Ground Improvement*, ed. H. Khabbaz, Z. Hossain, B. H. Nam, and X. Chen (Reston, VA: American Society of Civil Engineers, 2016), 44–51.
32. F. Radjai, M. Jean, J.-J. Moreau, and S. Roux, "Force Distributions in Dense Two-Dimensional Granular Systems," *Physical Review Letters* 77, no. 2 (1996): 274–277, https://doi.org/10.1103/PhysRevLett.77.274